Int J Earth Sci (Geol Rundsch)
DOI 10.1007/s00531-008-0397-x

ORIGINAL PAPER

# Exhumation processes during post-collisional stage in the Variscan belt revealed by detailed $^{40}Ar/^{39}Ar$ study (Tanneron Massif, SE France)

**Michel Corsini · V. Bosse · G. Féraud · A. Demoux · G. Crevola**

Received: 29 August 2007 / Accepted: 22 November 2008


**Abstract** Detailed $^{40}Ar/^{39}Ar$ geochronology on single grains of muscovite was performed in the Variscan Tanneron Massif (SE France) to determine the precise timing of the post-collisional exhumation processes. Thirty-two plateau ages, obtained on metamorphic and magmatic rocks sampled along an east–west transect through the massif, vary from 302 ± 2 to 321 ± 2 Ma, and reveal a heterogeneous exhumation of the lower crust that lasted about 20 Ma during late Carboniferous. In the eastern part of the massif, the closure of the K–Ar isotopic system is at 311–315 Ma, whereas in the middle part of the massif it closes earlier at 317–321 Ma. These cooling paths are likely to be the result of differential exhumation processes of distinct crustal blocks controlled by a major ductile fault, the La Moure fault that separates both domains. In the western part of the massif, the ages decrease from 318 to 303 Ma approaching the Rouet granite, which provides the youngest age at 303.6 ± 1.2 Ma. This age distribution can be explained by the occurrence of a thermal structure spatially associated to the magmatic complex. These ages argue in favour of a cooling of the magmatic body at around 15 Ma after the country rocks in the western Tanneron. The emplacement of the Rouet granite in the core of an antiform is responsible for recrystallization and post-isotopic closure disturbances of the K–Ar chronometer in the muscovite from the host rocks. These new $^{40}Ar/^{39}Ar$ ages clearly outline that at least two different processes may contribute to the exhumation of the lower crust in the later stage of collision. During the first stage between 320 and 310 Ma, the differential motion of tectonic blocks limited by ductile shear zones controls the post-collisional exhumation. This event could be related to orogen parallel shearing associated with crustal-scale strike-slip faults and regional folding. The final exhumation stages at around 300 Ma take place within the tectonic doming associated to magmatic intrusions in the core of antiformal structures. Local ductile to brittle normal faulting is coeval to Upper Carboniferous intracontinental basins opening.

**Keywords** Variscan · $^{40}Ar/^{39}Ar$ · Thermal doming · Exhumation · Tanneron Massif

M. Corsini (✉) · G. Féraud
Géosciences Azur (UMR-CNRS 6526), Nice-Sophia Antipolis University, Campus Valrose, 06 108 Nice Cedex, France
e-mail: corsini@unice.fr

V. Bosse
Laboratoire Magmas Volcans (UMR-CNRS 6524), Blaise Pascal University, Clermont-Ferrand, France

A. Demoux
Institut für Geowissenschaften, Mainz University, Mainz, Germany

G. Crevola
Institut EGID, Bordeaux III University, Pessac, France

## Introduction

Final stages of collisional mountain belts are characterized by thermal and mechanic equilibration of the thickened continental lithosphere. The timing and processes of exhumation of deep crust are still under debate and several mechanisms are currently considered: isostatic uplift, erosion, extensional tectonic, delamination or convective removal of the mantle part of the lithosphere. Because petrological, structural and kinematic descriptions are essential informations for the understanding of these processes, precise age data on rocks affected by these late events may significantly advance the discussion about the

Published online: 16 December 2008

exhumation model. Notably $^{40}Ar/^{39}Ar$ geochronology on single minerals allows determining the approximate cooling rates, which is a relevant parameter characterizing orogenic exhumation rate.

In the Variscan belt of Europe, late exhumation processes have been extensively studied without any general agreement. These are thought to be mainly associated with core complex-type structures, crustal-scale strike-slip faults and intracontinental basin formation (Burg et al. 1994; Costa and Rey 1995; Echtler and Malavielle 1990; Faure 1995; Faure et al. 2002; Gardien et al. 1997; Malavieille 1993; Soula et al. 2001). In this study, detailed $^{40}Ar/^{39}Ar$ geochronology on muscovite associated with structural study was conducted in the Maures-Tanneron Massif (SE France) to characterize the exhumation process of the lower crust during the late stages of the collision. The Maures-Tanneron Massif is the southernmost segment of the European Variscan belt in association with the external massifs of Argentera in the Southern Alps, Corsica and Sardinia (Matte 2001). This massif was chosen because it displays continuous exposures of quite nearly fresh rocks compared to other massifs of the Variscan belt, and few petrological, structural and geochronological data were available at the beginning of the study.

## Lithological and structural frameworks of the Tanneron Massif

### Lithological frameworks

Located in Southeastern France, the Maures-Tanneron Massif belongs to the Variscan Provence, limited by the Mediterranean sea to the South East (Fig. 1). The northern Tanneron Massif is separated from the Maures Massif by an E–W trending Permian basin. The whole massif records a polyphased deformation history of a high-grade metamorphism before Upper Carboniferous times (Crevola and Pupin 1994, and references therein). The Maures Massif (Fig. 1b) is separated in two main domains by the N–S trending Grimaud fault: (1) the Western and Central Maures are composed of Lower Palaeozoic metasediments (Western metamorphic unit), Precambrian to Lower Palaeozoic metasediments and metagranites (Bormes unit) and

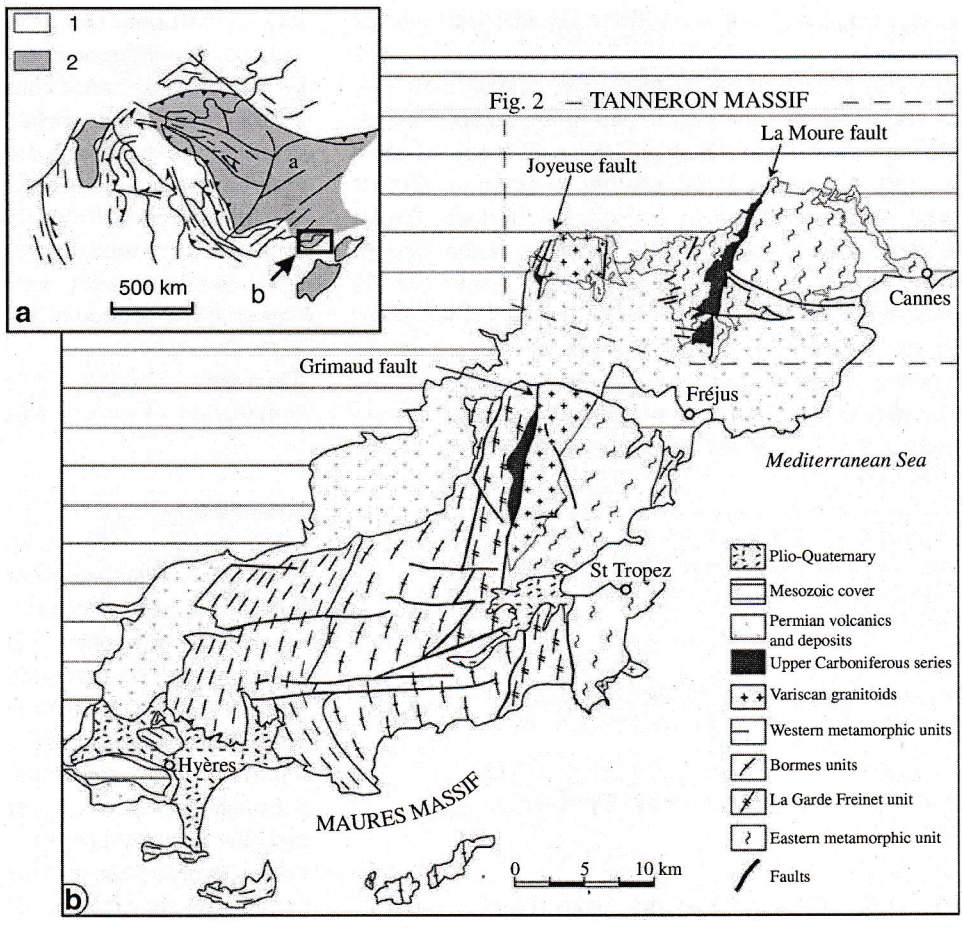


**Fig. 1** **a** General sketch map of the Variscan units in western Europe modified from Matte (2001): *1* external zones, *2* internal zones. **b** Structural sketch map of the Maures et Tanneron Massifs modified from Crevola and Pupin (1994)

a layered leptyno-amphibolic complex of Cambrian–Ordovician age (Innocent et al. 2003) associated with orthogneisses and micaschists of unknown age (La Garde-Freinet unit) and (2) the Eastern Maures mostly composed of granites and migmatitic para- and orthogneisses along with amphibolites containing relics of eclogite. The Tanneron Massif extending E–W over about 600 $km^2$ (Figs. 1b, 2) is mainly composed by micaschists, migmatitic para- and orthogneisses, amphibolites containing relics of eclogite and late granitic and tonalitic intrusions (Crevola et al. 1991; Crevola in Toutin-Morin et al. 1994). The metamorphic evolution of the Maures-Tanneron Massif (Seyler 1975; Maquil 1976; Le Marrec 1976; Crevola 1977; Bard and Caruba 1981, 1982; Caruba 1983; Bouloton et al. 1998; Buscail and Leyreloup 1999; Bellot et al. 2003) is characterized by (1) an early HP–LT eclogitic stage, (2) a MP–MT barrovian main stage and (3) a late HT–LP stage. During the main barrovian stage the anatexis is reached in the sillimanite–muscovite zone, which spread over the Eastern Maures and the whole Tanneron Massif. Successive tectono-metamorphic events reflect subduction, collision and late exhumation of a previously thickened crust.

Structural pattern

Previous structural analyses of the Maures-Tanneron Massif (Arthaud and Matte 1966; Seyler 1982, Crevola 1977; Caruba 1983; Vauchez and Bufalo 1985, 1988; Morillon 1997; Buscail 2000; Bellot et al. 2000, 2002) indicate a polyphase deformation with four main phases. The first two phases of pervasive ductile deformation (D1–D2) are characterized by isoclinal and sheath folds with penetrative flat lying foliation, S1–S2, and horizontal stretching and mineral lineations, L1–L2. The D1 deformational phase is characterized by WNW directed thrusting mostly found in Western and Central Maures. The D2 deformational phase is observed in Central and Eastern Maures and in the whole Tanneron where the deformation is marked at all scales by isoclinal folds with prominent orogen parallel stretching lineation, and is developed during transpressional deformation in a regime of decreasing pressure. The third deformation event (D3) is characterized by orogen parallel shearing with N–S trending sinistral ductile strike-slip shear zones associated to large-scale concentric folds and axial planar cleavage (S3–L3). The last phase of deformation (D4) varies from ductile to brittle regimes, and is characterized by dextral strike-slip shearing, granite and tonalite emplacement and normal faulting associated with the Upper Carboniferous basin opening during progressive exhumation of the crust.

In the Tanneron Massif, two steeply dipping N–S trending ductile to brittle faults, so-called the Joyeuse and La Moure faults limiting elongate Stephanian sedimentary basins, divide the massif into three domains (Figs. 1, 2): the Western Tanneron, west of the Joyeuse fault; the Eastern Tanneron, east of the La Moure fault; and the Middle Tanneron between them. Through out the massif, the metamorphic rocks are characterized by a well-developed foliation related to the D1–D2 phases. Three large kilometric folding structures (D3) are distinguished from W to E (Fig. 4): the Rouet antiform, the Reyran synform and the Cannes antiform (Crevola and Pupin 1994). In the most western part, near the Joyeuse fault, the metamorphic pile is intruded by a magmatic complex: the calk-alkaline Prignonet tonalite of mixed mantle–crust origin at first, and then the younger syntectonic peraluminous Rouet granite of deep crustal origin (Onezime et al. 1999, Fig. 2). In this area, the metamorphic foliation of the sillimanite–cordierite rich migmatitic gneiss displays a cartographic dome-like structure all around the tonalite–granite complex (Crevola in Toutin-Morin et al. 1994; Corsini et al. 2004a; Demoux et al. 2008). At the western border of the dome structure, the narrow Pennafort Stephanian detrital basin (Fig. 2) lies unconformably on the mylonitic gneisses and is in tectonic contact with the country gneiss to the east by the Joyeuse fault. The hanging wall of the Joyeuse fault is characterized by steep mylonitic foliation planes associated to steeply dipping stretching lineations. The shear criteria indicate a top to the SW displacement, assuming a normal ductile shearing. The magmatic fabric of the tonalite is parallel to the tectonic fabric of the surrounding gneisses, suggesting a coeval emplacement of the magmatic complex. The normal faulting represents the last deformation stage, varying from ductile to brittle condition, associated to folding, granitic intrusion and intracontinental basin emplacement.

## Previous geochronological data on the Southern European Variscan belt

Previously obtained ages in the Maures Massif are high pressure (HP) metamorphism at 431 ± 4 Ma (U–Pb zircon in eclogite, Moussavou 1998), followed by decompression and partial melting between 350 and 330 Ma (345 ± 3 Ma, U–Pb monazite in migmatitic orthogneiss: Moussavou 1998; 348 ± 7 Ma, Rb–Sr whole rock: Innocent et al. 2003; 338 ± 8, 333 ± 4 and 324 ± 5 Ma on intrusives, U–Pb zircon: Moussavou 1998). In the Tanneron Massif, ages from 440 to 410 Ma recorded in an orthogneiss from the central part of the massif are related to the subduction stage (U–Pb on monazite; Demoux et al. 2008). Ages at 317 ± 1 Ma in the central part, and at 309 ± 5 and 310 ± 2 Ma in the eastern part of the massif correspond to a HT metamorphism event (U–Pb on

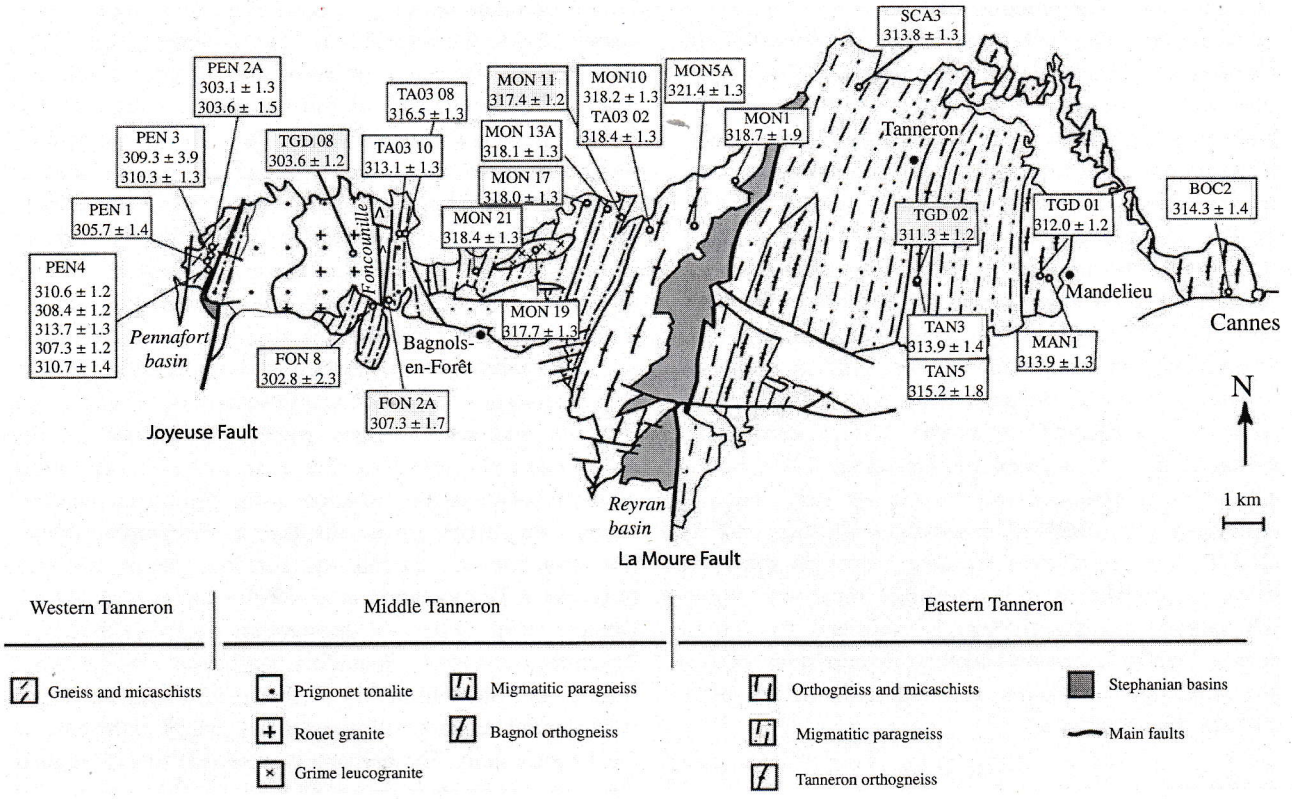


**Fig. 2** Geological sketch map modified after Crevola and Pupin (1994) showing the structural divisions of the Tanneron Massif and the location of the studied samples. The $^{40}Ar/^{39}Ar$ ages are shown at the $2\sigma$ level

monazite; Demoux et al. 2008). A Rb–Sr whole rock isochron age at 374 ± 25 Ma is also recorded in gneisses from the Tanneron Massif (recalculated with decay constants recommended by Steiger and Jäger 1977; Roubault et al. 1970).

In the Maures Massif, the cooling history was recently reconstructed from $^{40}Ar/^{39}Ar$ dating on amphiboles, biotites and muscovites (Morillon et al. 2000; Buscail 2000). $^{40}Ar/^{39}Ar$ muscovite and biotite plateau ages of 317.2 ± 1.0–322.9 ± 1.7 Ma on the western side of the Grimaud fault contrast with those of 300.2 ± 0.6–306 ± 2.4 Ma on the eastern side, and demonstrate distinct cooling history on both sides of the fault (Morillon et al. 2000, Fig. 6). In the same way, amphiboles from the western side have $^{40}Ar/^{39}Ar$ plateau ages from 328.1 ± 2.8 to 329.9 ± 2.1 Ma, whereas on the eastern side amphiboles have $^{40}Ar/^{39}Ar$ plateau ages from 307.9 ± 1.2 to 317.4 ± 2.4 Ma. Morillon et al. (2000) proposed this East–West age difference as the result of diachronic stages of exhumation along the Grimaud fault.

Late to post-kinematic granites are present in the Tanneron and in the Maures Massifs. The Plan-de-la-Tour granite (Maures Massif) and the Rouet granite (Tanneron Massif) yielded whole rock Rb–Sr ages of 314 ± 10 Ma (recalculated, Roubault et al. 1970). The Plan-de-la-Tour granite gave a whole rock Rb–Sr age of 313 ± 10 Ma (recalculated, Maluski 1972) and a U–Pb zircon age of 324 ± 5 Ma (Moussavou 1998), whereas in the Tanneron Massif the emplacement of the Rouet granite is dated at 302 ± 4 Ma (U–Pb on monazite; Demoux et al. 2008). Tonalite bodies yielded a U–Pb zircon age of 334 ± 3 Ma (Moussavou 1998) in the Maures Massif and a whole rock K–Ar age of 322 ± 10 Ma (recalculated according to Dalrymple 1979; Roubault et al. 1970) in the Tanneron Massif. The later stage is contemporaneous with the deposition of Stephanian detrital sediments.

Multistage tectonic evolution is found all along the Variscan belt. In the External Massif of Argentera, geochronological studies gave evidences to the following tectono-metamorphic evolution (1) HP/HT events at ca. 424 ± 4 Ma (U–Pb zircon age, Paquette et al. 1989), (2) amphibolite facies metamorphism and anatexis at 323 ± 12 Ma (U–Pb zircon age, Rubatto et al. 2001), (3) LP/HT metamorphism at ca. 310–315 Ma ($^{40}Ar/^{39}Ar$, Corsini et al. 2004a) and (4) emplacement of the Argentera granite and subsequent melting at ca. 296–299 Ma ($^{40}Ar/^{39}Ar$, Monié and Maluski 1983; Corsini et al. 2004b). In western Corsica, four post-collisional magmatism events

**Table 1** Lithologies of dated samples

| Samples | Lithology | Plateau age ($2\sigma$) | $^{39}$Ar (%) |
|---|---|---|---|
| Eastern Tanneron | | | |
| BOC 2 | Pegmatitic vein | 314.3 ± 1.4 | 100 |
| TGD 01 | Pegmatitic vein | 312.0 ± 1.2 | 92.1 |
| MAN 1 | Pegmatitic vein | 313.9 ± 1.3 | 100 |
| TGD 02 | Orthogneiss | 311.3 ± 1.2 | 87.5 |
| TAN 3 | Orthogneiss | 313.9 ± 1.4 | 84.1 |
| TAN 5 | Orthogneiss | 315.2 ± 1.8 | 100 |
| SCA 3 | Biotitic gneiss | 313.8 ± 1.3 | 97.3 |
| Middle Tanneron | | | |
| FON 2A | Paragneiss | 307.3 ± 1.7 | 80.9 |
| FON 8 | Aplitic vein | 302.8 ± 2.3 | 77.9 |
| TA03 08 | Paragneiss | 316.5 ± 1.3 | 98.1 |
| TA03 10 | Paragneiss | 313.1 ± 1.3 | 80.7 |
| TGD 08 | Granite | 303.6 ± 1.2 | 92.9 |
| MON 1 | Orthogneiss | 318.7 ± 1.9 | 93.3 |
| | | 320.1 ± 1.4 | 98.6 |
| MON 5A | Orthogneiss | 321.4 ± 1.1 | 87.3 |
| MON 10 | Orthogneiss | 318.2 ± 1.3 | 92.1 |
| TA03 02 | Orthogneiss | 318.4 ± 1.3 | 97.1 |
| MON 11 | Paragneiss | 317.4 ± 1.3 | 87.6 |
| MON 13A | Migmatitic paragneiss | 318.1 ± 1.3 | 65.2 |
| MON 17 | Paragneiss | 318.0 ± 1.3 | 73.2 |
| MON 19 | Leucogranite | 317.7 ± 1,3 | 92.6 |
| MON 21 | Pegmatitic vein | 318.4 ± 1.3 | 100 |
| Western Tanneron | | | |
| PEN 1 | Pegmatitic vein | 305.7 ± 1.4 | 91.8 |
| PEN 2A | Pegmatitic vein | 303.6 ± 1.5 | 96.6 |
| | | 303.1 ± 1.2 | 90.4 |
| PEN 3 | Micaschist | 310.3 ± 1.2 | 94.1 |
| | | 309.3 ± 3.9 | 89.3 |
| PEN 4 | Micaschist | 307.3 ± 1.2 | 87.5 |
| | | 310.6 ± 1.2 | 84.8 |
| | | 308.4 ± 1.2 | 84.7 |
| | | 313.7 ± 1.3 | 87.1 |
| | | 310.7 ± 1.4 | 83.4 |

All isotopic measurements are corrected for K and Ca isotopic interferences

were recognized by U–Pb zircon dating, respectively at 345, 338, 305 and 280 Ma with a contribution of mantle materials triggering partial melting in the lower crust (Paquette et al. 2003). In Sardinia geochronological dating allows to recognize (1) MP–MT metamorphism reflecting the end of thickening stage at 344 ± 7 Ma (whole rock Rb–Sr on migmatite, Ferrara et al. 1978), (2) retrograde metamorphism at 320–300 Ma ($^{40}$Ar/$^{39}$Ar on muscovite, Di Vincenzo et al. 2004) and emplacement of anatectic granitoids at ca. 290–310 Ma (whole rock Rb–Sr, Del Moro et al. 1975).

From these geochronological data, it is abundantly clear that all these massifs forming the Southern European Variscan belt present a polyphase metamorphic evolution characterized by (1) HP metamorphism related to early stages of burial at ca. 420 Ma, (2) barrovian metamorphism and anatexis associated with crustal thickening at ca. 350 Ma and (3) HT metamorphic conditions and abundant magmatism related to the late exhumation processes between 330 and 300 Ma.

## Analytical method

Samples of different lithologies (para- and orthogneisses, micaschists, pegmatitic or aplitic veins, granite) were collected in the Tanneron Massif for detailed $^{40}$Ar/$^{39}$Ar analyses on muscovite (see Table 1 for details). Mineral separates were obtained after crushing and handpicking of single grains ranging from 0.5 to 1 mm. $^{40}$Ar/$^{39}$Ar data were obtained in Geosciences Azur laboratory at the Nice-Sophia Antipolis University. Carefully selected muscovite single grains were irradiated in the nuclear reactor of the McMaster University in Hamilton, Canada, in position 5c. The total neutron flux density during irradiation was $8.8 \times 10^{18}$ n cm$^{-2}$ with a maximum flux gradient estimated with a precision of ±0.2% in the volume, where the samples were included. Hb3gr hornblende was used as neutron fluence monitor. We calculated *J*-values relative to an age of Hb3gr of 1072 Ma (Turner et al. 1971; Roddick 1983) and using the decay constants of Steiger and Jäger (1977). The step-heating procedure used in this study is described in detail by Ruffet et al. (1991). The heating was carried out by a $CO_2$ Synrad 48-5 laser and isotopic measurements were performed by a VG 3600 mass spectrometer working with a Daly detector system. The blanks of the extraction and purification laser system were measured every third step and subtracted from each argon isotope from the subsequent gas fraction. Typical blank values were in the range of 6–18, 0.3–2.0, 0.4–1.2 and 0.6–1.4 $\times 10^{-13}$ccSTP for the mass 40, 39, 37 and 36, respectively. The criteria for defining plateau ages were as follows: (1) a plateau age should contain at least 70% of released $^{39}$Ar; (2) there should be at least three successive steps in the plateau; and (3) the integrated age of the plateau should agree with each apparent age of the plateau within a $2\sigma$ error confidence interval. Apparent ages are quoted to the $1\sigma$ level on Figs. 3 and 4, when plateau ages are given at the $2\sigma$ level and do not include the errors on the age of the monitor.

The error on the $^{40}$Ar*/$^{39}$Ar$_k$ ratio of the monitor is included in the plateau age error bar calculation.

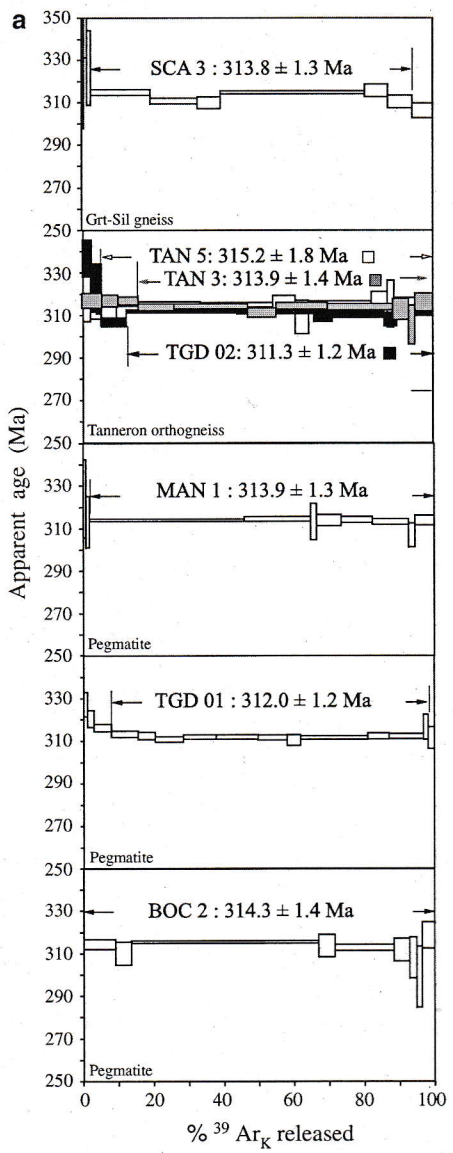


**Fig. 3** **a** $^{40}Ar/^{39}Ar$ age spectra on muscovite single grains in samples from the eastern Tanneron. The *numbers* indicate plateau ages with error bars at the $2\sigma$ level. Apparent ages are given at the $1\sigma$ level. **b** $^{40}Ar/^{39}Ar$ age spectra on muscovite single grains in samples from the middle Tanneron. The *numbers* indicate plateau ages with *error bars* at the $2\sigma$ level. Apparent ages are given at the $1\sigma$ level. **c** $^{40}Ar/^{39}Ar$ age spectra on muscovite single grains in samples from the western Tanneron. The *numbers* indicate plateau ages with *error bars* at the $2\sigma$ level. Apparent ages are given at the $1\sigma$ level

## Samples description and $^{40}Ar/^{39}Ar$ results

A total of 25 samples from various lithologies were collected from east to west in the Tanneron Massif. The maximum temperature during the peak of metamorphism is above the stability domain of muscovite in the eastern and the middle Tanneron domains. Thus, muscovite in these studied samples is mainly retrograde, replacing the high temperature paragenesis. The muscovite compositions correspond to pure muscovite (Si between 6.1 and 6.3) and compositional variations are limited (Table 2). In the micaschists from the western Tanneron (e.g. PEN 4), large primary muscovites are strongly deformed and reveal recrystallized domains on the rim of the grains. Small neocrystallized muscovites are also present. In these samples, muscovites also display limited variations of the Si content (Table 2).

### $^{40}Ar/^{39}Ar$ data from the Eastern Tanneron

Muscovite single grains were analysed in seven samples from the eastern part of the Tanneron Massif (Figs. 2, 3a; Table 1). Plateau ages from this part of the Tanneron Massif are clustered, ranging from 311.3 ± 1.3 to 315.2 ± 1.8 Ma, although the analysed muscovites originate from different types of rocks. Samples BOC 2, MAN 1 and TGD 01 are pegmatitic veins (with quartz, K-feldspar, plagioclase, biotite, rare garnet and muscovite) crosscutting the main foliation in granitic orthogneisses (BOC 2) or micaschists (MAN 1 and TGD 01). No deformation is observed in these samples. Muscovites from BOC 2, MAN 1 and TGD 01 yield similar plateau ages of 314.3 ± 1.4, 313.9 ± 1.3 and 312.0 ± 1.2 Ma, respectively. In the Tanneron orthogneiss, three samples TAN 3, TAN 5 and TGD 02 were analysed. This granitic orthogneiss displays different stages of preservation, from original granite (TAN 5) to mylonitic and migmatitic orthogneiss (TAN 3, TGD 02). The mylonitic deformation is characterized by decrease of the grain size, well-developed biotite and muscovite foliation and strongly elongated quartz grains parallel to the lineation. Magmatic mineral assemblages (quartz, plagioclase, K-felspar, biotite and garnet) are nevertheless sometimes preserved. Large muscovite grains located in the foliation give plateau ages of 313.9 ± 1.4, 315.2 ± 1.8 and 311.3 ± 1.2 Ma in the samples TAN 3, TAN 5 and TGD 02, respectively. In the northern part of the eastern Tanneron, the sample SCA 3 is a highly deformed biotitic gneiss with relictual garnet, plagioclase and abundant sillimanite. A late muscovite grain located in the foliation with biotite displays a plateau age of 313.8 ± 1.3 Ma.

### $^{40}Ar/^{39}Ar$ data from the Middle Tanneron

Fourteen samples from different lithologies are located between the La Moure and the Joyeuse faults (Figs. 2, 3b; Table 1). Samples MON 1, MON 5A, MON 10 and TA 03–02 were collected in the Bois de Bagnols orthogneiss (dark gneiss with abundant biotite). Muscovites associated with chloritized biotites in the foliation from the samples MON 1, MON 10 and TA 03–02 yield similar plateau ages

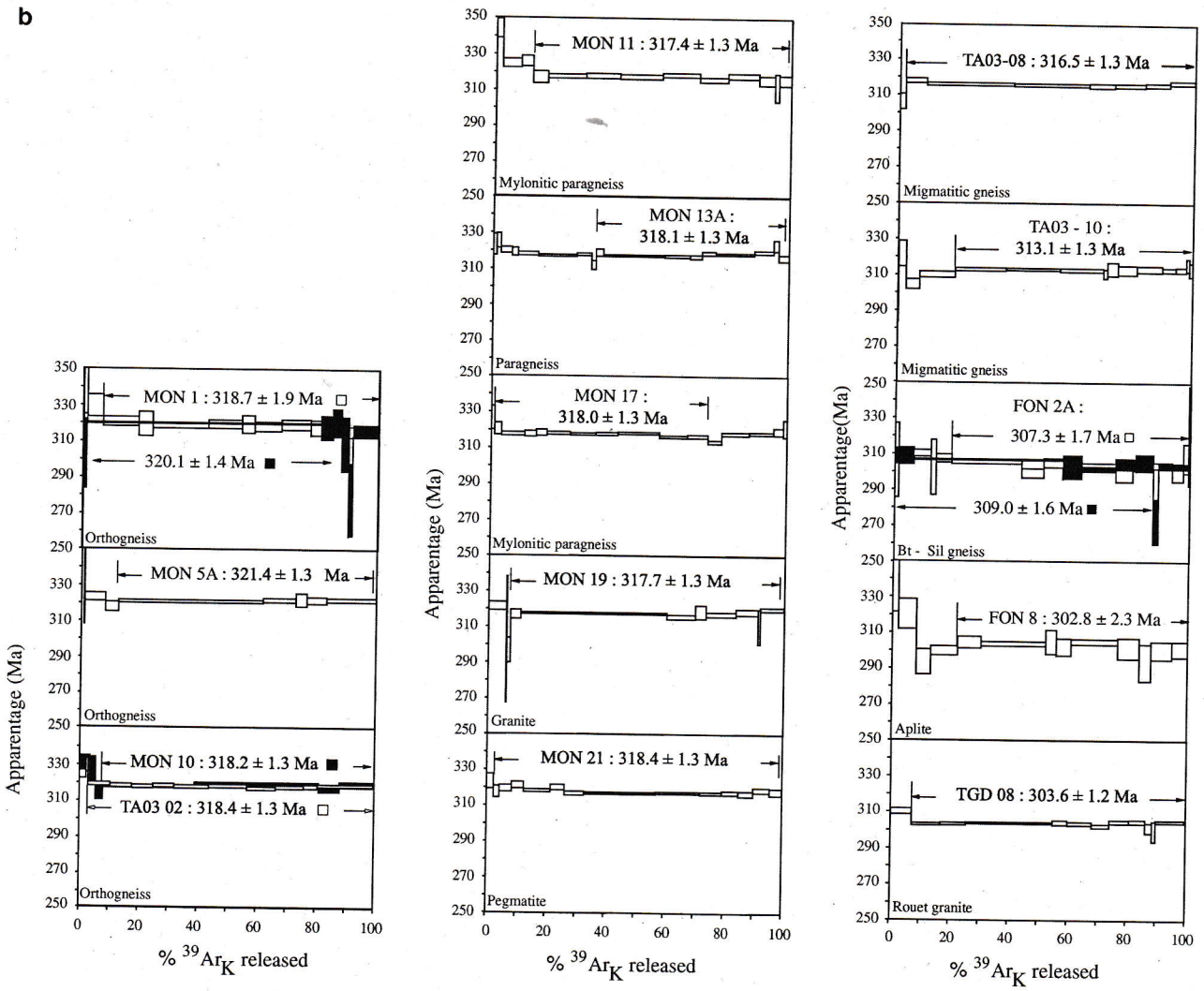


**Fig. 3** continued

of 318.7 ± 1.9, 318.2 ± 1.3 and 318.4 ± 1.3 Ma, respectively. Duplicated muscovite from the micaschist MON 1 gives consistent plateau age of 320.1 ± 1.4 Ma. The plateau age of the MON 5A sample is slightly older at 321.4 ± 1.3 Ma. West of the Bois de Bagnols orthogneiss, migmatitic paragneisses are abundant (Fig. 2). In this area sillimanite paragneisses MON 11 and MON 17 yield consistent plateau ages of 317.4 ± 1.3 and 318.0 ± 1.3 Ma. MON 13A (migmatitic gneiss) does not display a plateau age, because of a discordant apparent age given by the step number 8, representing only 1.5% of the total $^{39}Ar$ released. Nevertheless, a weighted mean age of 318.1 ± 1.3 Ma, calculated over 65.2% of $^{39}Ar$ is consistent with the previous mentioned plateau ages, and is therefore probably valid. Muscovite from the leucogranite MON 19 and pegmatite MON 21 give also consistent plateau ages of 317.7 ± 1.3 and 318.4 ± 1.3. Ma.

Going to the east, magmatic and metamorphic rocks display younger plateau ages. Muscovite from the Rouet granite TGD 08 gives a plateau age of 303.6 ± 1.2 Ma. A young age of 302.8 ± 2.3 Ma were also displayed by a muscovite from a slightly deformed aplitic vein (FON 8). In the paragneisses TA 03–08 and TA 03–10 muscovites associated with chloritized biotite and K-felspar show plateau ages of 316.5 ± 1.3 and 313.1 ± 1.3 Ma, respectively. In the paragneiss FON 2A, duplicated muscovites display similar plateau ages of 307.3 ± 1.7 and 309.0 ± 1.6 Ma. It should be noted that muscovites display subtly disturbed age spectra in the metamorphic samples, even though they are within the 2$\sigma$ of the plateau ages. For example, muscovite TA 03–10 yields an age spectrum with younger ages at low temperature steps suggesting a slight radiogenic $^{40}Ar$ loss. Muscovite TA 03–08 yields a slightly saddle-shaped age spectrum and

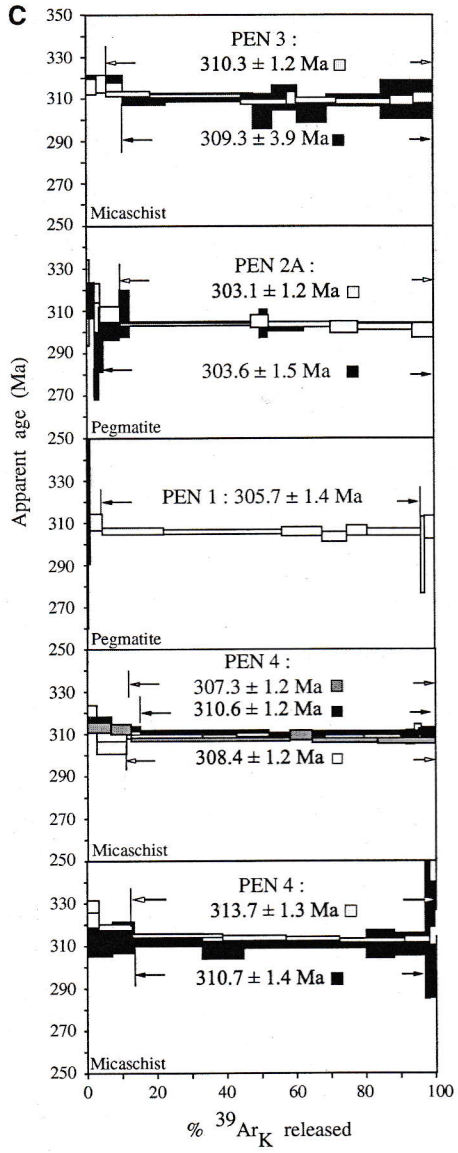


**Fig. 3** continued

duplicates of sample FON 2A display age spectra with decreasing ages towards high temperature steps. These age spectra shapes suggest post-isotopic closure disturbances of the analysed muscovites, which will be discussed further.

### $^{40}Ar/^{39}Ar$ data from the Western Tanneron

Four samples collected west of the Joyeuse fault were analysed (Fig. 3c; Table 1). Muscovites from slightly deformed pegmatites crosscutting the micaschists yield consistent duplicated plateau ages of 303.1 ± 1.3 and 303.6 ± 1.5 Ma in the sample PEN 2A and 305.7 ± 1.4 Ma in the sample PEN 1. In the biotite–muscovite micaschist PEN 3, two duplicated muscovites yield consistent plateau ages of 310.3 ± 1.3 and 309.3 ± 3.9 Ma, even though they display slightly saddle-shaped age spectra. Five duplicated muscovites from the micaschist PEN 4 give discrepant plateau ages of 307.3 ± 1.2, 310.6 ± 1.2, 308.4 ± 1.2, 313.7 ± 1.3 and 310.7 ± 1.4 Ma, an age variation of ~6 Ma or 2%. Some of these age spectra yield decreasing ages towards high temperature steps (Fig. 3c).

## Discussion

Thirty-two $^{40}Ar/^{39}Ar$ plateau ages ranging from 302 ± 2 to 321 ± 2 Ma were obtained on single grains of muscovite from 25 metamorphic and magmatic rocks from the Tanneron Massif. Only one sample (MON 13A) did not display a plateau age following the previously described criteria, but a probably valid weighted mean age, consistent with plateau ages obtained on the same area (see above). These ages show a good internal reproducibility (except the sample PEN 4 which will be discussed below) whatever the lithology (metamorphic and magmatic rocks) and the metamorphic grade.

There is an excellent agreement with previous age data (Morillon et al. 2000) from 322.9 ± 1.7 to 300.2 ± 0.6 Ma obtained in the southern Maures Massif, demonstrating the similar metamorphic evolution of the two massifs. Therefore, the observed age distribution throughout the massif provides robust constraints on its late thermal evolution, and shows an inhomogeneous exhumation and cooling of the whole Tanneron Massif. The closure temperature of the K–Ar system in white micas will be considered here to fall in the range of 350–450°C (Villa 1998; Mulch et al. 2002). Although this temperature is still debated, this is not the purpose of this study to determine the temperature of the isotopic closure in muscovite.

### Thermal evolution around the La Moure fault

Considering the $^{40}Ar/^{39}Ar$ plateau age distribution throughout the Tanneron Massif (Fig. 2) it appears that this distribution may correspond to the structural division by the La Moure and the Joyeuse faults. On both sides of the La Moure fault, the ages are clearly different. In the eastern Tanneron, the age distribution is homogeneous, ranging from 311.3 ± 1.2 to 315.2 ± 1.8 Ma, with a mean age of ca. 313 Ma (Figs. 2, 5, 6). West of the La Moure fault, the ages are significantly older, between 321.4 ± 1.3 (MON 5A) and 318.4 ± 1.3 Ma (MON 21) and the age distribution is also homogeneous at least over a distance of 8 km west of the La Moure fault with a mean age of ca. 318 Ma (Figs. 2, 4, 5). The age difference between the eastern and the middle Tanneron suggests that the La Moure fault has played an important role during the exhumation of these

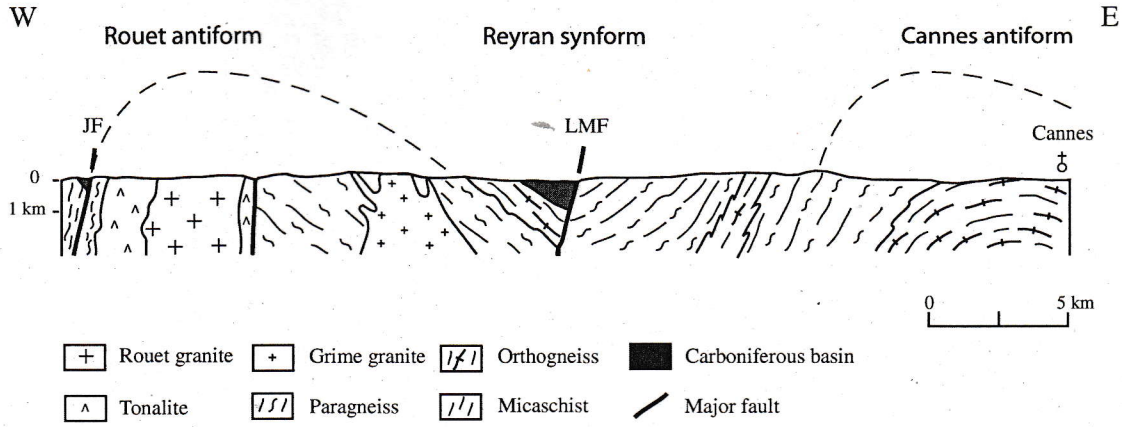


**Fig. 4** Geological cross section showing the structural division of the Tanneron Massif and the intrusion of the Rouet magmatic complex into the core of the Rouet antiform (modified after Crevola and Pupin 1994) *JF* Joyeuse fault, *LMf* La Moure fault

two domains. The eastern part of the Tanneron has reached the 350–450°C temperature interval (closure of the K–Ar isotopic system in muscovite) at around 311–315 Ma, e.g. around 5 Ma later than the middle part of the Tanneron. These muscovite $^{40}Ar/^{39}Ar$ ages are in agreement with the paleontological study in the same area. In the Reyran basin, the age of the sedimentation of the sandstones, reworking pebbles of the metamorphic basement, is estimated Upper Westphalian–Lower Stephanian based on paleo-flora (Basso 1985). Therefore, the basement of the Tanneron Massif, west of La Moure Fault, was subjected to erosion at around 305 Ma (Odin and Odin 1990). Assuming a mean geotherm of 30°C/km, the exhumation rate can be estimated at around 1 mm/year in this area. Such a rapid exhumation of the basement testifies the role of the La Moure fault characterized at map scale by a linear trace and a steep shear plane (Figs. 1, 2, 4).

## Age distribution around the Joyeuse fault

In contrast with the area of the La Moure fault, the age distribution around the Joyeuse fault is not in agreement with the structural division of the massif, e.g. crustal blocks separated by ductile faults. No age difference is found on both sides of the Joyeuse fault (Fig. 2). East of the Joyeuse fault, (in the western part of the middle Tanneron) the muscovite ages are decreasing going to the west from 316.5 ± 1.3 to 302.8 ± 2.3 Ma. West of the Joyeuse fault, in the limited area between the Joyeuse fault and the Mesozoic series, the plateau ages vary in the same range as East of the fault, from 310.7 ± 1.4 to 303.1 ± 1.3 Ma (Fig. 3c). These results contrast with those obtained in the Maures Massif by Morillon et al. (2000) on both sides of the Grimaud fault which is usually interpreted as the extension of the Joyeuse fault in the Maures Massif (Onezime et al. 1999). In the Maures Massif, the $^{40}Ar/^{39}Ar$ data on muscovite, biotite and amphibole show distinct cooling histories between 330 and 300 Ma on both sides of the Grimaud fault. The Grimaud fault is thus interpreted by Morillon et al. (2000) as a major crustal fault, which controls the exhumation of two crustal blocks. In the Tanneron Massif, such distinct cooling histories based on $^{40}Ar/^{39}Ar$ data cannot be found, suggesting a more complex role of the Joyeuse fault during the cooling of this part of the massif.

## Consequences on the interpretation of the $^{40}Ar/^{39}Ar$ ages

On both sides of the Joyeuse fault, the $^{40}Ar/^{39}Ar$ ages are regularly scattered between 318 and 303 Ma (Fig. 5). The age scattering is significantly higher than the error margins of the calculated plateau ages, even in the same sample, and thus should have a geological significance. Even though they allow plateau age calculation, muscovite $^{40}Ar/^{39}Ar$ ages around the Joyeuse fault give saddle and staircase shaped spectra, which have been interpreted by many authors as the result of mixing of inherited and neocrystallized white micas due to partial recrystallization (Dunlap et al. 1991; Dunlap 1997; Cheilletz et al. 1999; Castonguay et al. 2001; Alexandrov et al. 2002) rather than excess argon component (McDougall and Harrison 1999). Dunlap et al. (1991) and Cheilletz et al. (1999) argued that the saddle-shaped age spectra could result from the mixing of mineral phases, e.g. inherited versus recrystallized muscovite, during intense deformation. Castonguay et al. (2001) give the same interpretation to explain the scattering of the muscovite $^{40}Ar/^{39}Ar$ ages and the spectra shapes in metamorphic rocks, but in their study the recrystallized phases (e.g. muscovite) have the same composition that the inherited ones. Thus, the recrystallized muscovites do not display any core–rim chemical variation. Alexandrov et al.

**Table 2** Representative muscovite composition

| Sample | BOC 2 | Pegmatite | MAN 1 | Pegmatite | TAN 3 | Orthogneiss | SCA 3 | Paragneiss | TAN 5 | Orthogneiss | TA 03-10 | Paragneiss | PEN 4 | Micaschiste | PEN 4 | Micaschiste | FON 2A | Paragneiss |
|---|---|---|---|---|---|---|---|---|---|---|---|---|---|---|---|---|---|---|
| Anal. no | 333 | 334 | 365 | 366 | 22 | 23 | 278 | 279 | 157 | 158 | 2 | 3 | 9 | 10 | 15 | 20 | 23 | 24 |
| | core | rim | core | rim | core | rim | core | rim | ms core | ms rim | core | rim | core | rim | core | small grain | core | rim |
| $SiO_2$ | 45.02 | 45.33 | 45.69 | 45.48 | 45.65 | 45.87 | 45.37 | 45.59 | 45.37 | 45.55 | 46.40 | 46.45 | 46.17 | 46.21 | 47.19 | 45.64 | 45.58 | 45.60 |
| $TiO_2$ | 0.25 | 0.17 | 0.23 | 0.18 | 1.07 | 1.30 | 0.95 | 1.24 | 1.35 | 1.17 | 0.89 | 0.85 | 1.13 | 1.05 | 0.76 | 0.53 | 1.66 | 1.37 |
| $Al_2O_3$ | 35.79 | 35.60 | 35.72 | 35.68 | 34.47 | 34.96 | 35.77 | 35.66 | 35.51 | 35.51 | 35.80 | 34.91 | 35.30 | 35.70 | 33.26 | 34.88 | 35.18 | 35.34 |
| $Cr_2O_3$ | 0.10 | 0.03 | 0.00 | 0.00 | 0.04 | 0.01 | 0.03 | 0.08 | 0.00 | 0.04 | 0.00 | 0.00 | 0.07 | 0.06 | 0.08 | 0.02 | 0.00 | 0.02 |
| FeO | 1.53 | 1.62 | 1.40 | 1.34 | 1.33 | 1.21 | 0.98 | 0.91 | 0.95 | 0.80 | 0.94 | 1.11 | 1.31 | 1.51 | 2.26 | 1.51 | 0.96 | 1.13 |
| MnO | 0.00 | 0.03 | 0.00 | 0.00 | 0.05 | 0.11 | 0.00 | 0.00 | 0.02 | 0.01 | 0.00 | 0.00 | 0.00 | 0.04 | 0.09 | 0.02 | 0.00 | 0.01 |
| MgO | 0.50 | 0.60 | 0.74 | 0.69 | 0.81 | 0.87 | 0.65 | 0.55 | 0.65 | 0.59 | 0.85 | 0.97 | 0.58 | 0.56 | 1.16 | 0.73 | 0.56 | 0.60 |
| CaO | 0.00 | 0.00 | 0.00 | 0.00 | 0.01 | 0.01 | 0.00 | 0.00 | 0.00 | 0.00 | 0.03 | 0.01 | 0.02 | 0.06 | 0.00 | 0.01 | 0.00 | 0.00 |
| $Na_2O$ | 0.70 | 0.62 | 0.68 | 0.59 | 0.35 | 0.33 | 0.58 | 0.81 | 0.40 | 0.37 | 0.37 | 0.36 | 0.67 | 0.71 | 0.37 | 0.55 | 0.61 | 0.59 |
| $K_2O$ | 10.72 | 11.21 | 10.42 | 10.81 | 10.97 | 10.83 | 10.63 | 10.38 | 11.13 | 11.11 | 10.42 | 10.29 | 9.82 | 9.86 | 9.87 | 10.49 | 10.47 | 10.35 |
| Total | 94.61 | 95.19 | 94.88 | 94.77 | 94.75 | 95.50 | 94.97 | 95.20 | 95.38 | 95.15 | 95.70 | 94.94 | 95.08 | 95.74 | 95.04 | 94.37 | 95.02 | 95.01 |
| $H_2O$ | 4.44 | 4.46 | 4.47 | 4.46 | 4.45 | 4.49 | 4.48 | 4.49 | 4.48 | 4.48 | 4.54 | 4.50 | 4.51 | 4.53 | 4.49 | 4.45 | 4.49 | 4.49 |
| Total | 99.06 | 99.65 | 99.35 | 99.23 | 99.20 | 99.99 | 99.45 | 99.70 | 99.86 | 99.63 | 100.24 | 99.44 | 99.59 | 100.28 | 99.53 | 98.83 | 99.51 | 99.50 |
| O | 22.000 | 22.000 | 22.000 | 22.000 | 22.000 | 22.000 | 22.000 | 22.000 | 22.000 | 22.000 | 22.000 | 22.000 | 22.000 | 22.000 | 22.000 | 22.000 | 22.000 | 22.000 |
| Si | 6.063 | 6.085 | 6.112 | 6.104 | 6.139 | 6.111 | 6.065 | 6.073 | 6.056 | 6.085 | 6.131 | 6.187 | 6.140 | 6.112 | 6.301 | 6.147 | 6.087 | 6.088 |
| Ti | 0.026 | 0.017 | 0.023 | 0.018 | 0.109 | 0.130 | 0.096 | 0.124 | 0.136 | 0.118 | 0.088 | 0.085 | 0.113 | 0.104 | 0.076 | 0.054 | 0.167 | 0.138 |
| Al | 5.681 | 5.632 | 5.631 | 5.644 | 5.462 | 5.489 | 5.635 | 5.598 | 5.586 | 5.590 | 5.574 | 5.479 | 5.532 | 5.564 | 5.233 | 5.535 | 5.535 | 5.560 |
| Cr | 0.010 | 0.003 | 0.000 | 0.000 | 0.004 | 0.001 | 0.003 | 0.008 | 0.000 | 0.004 | 0.000 | 0.000 | 0.007 | 0.006 | 0.009 | 0.002 | 0.000 | 0.002 |
| Fe | 0.172 | 0.181 | 0.157 | 0.150 | 0.150 | 0.135 | 0.110 | 0.101 | 0.106 | 0.089 | 0.104 | 0.124 | 0.146 | 0.167 | 0.252 | 0.170 | 0.107 | 0.126 |
| Mn | 0.000 | 0.003 | 0.000 | 0.000 | 0.006 | 0.013 | 0.000 | 0.000 | 0.002 | 0.001 | 0.000 | 0.000 | 0.000 | 0.004 | 0.010 | 0.002 | 0.000 | 0.001 |
| Mg | 0.101 | 0.120 | 0.148 | 0.138 | 0.163 | 0.173 | 0.130 | 0.109 | 0.130 | 0.118 | 0.168 | 0.192 | 0.115 | 0.110 | 0.232 | 0.147 | 0.111 | 0.120 |
| Ca | 0.000 | 0.000 | 0.000 | 0.000 | 0.001 | 0.001 | 0.000 | 0.000 | 0.000 | 0.000 | 0.004 | 0.002 | 0.003 | 0.008 | 0.000 | 0.001 | 0.000 | 0.000 |
| Na | 0.182 | 0.162 | 0.177 | 0.154 | 0.092 | 0.085 | 0.151 | 0.208 | 0.105 | 0.095 | 0.094 | 0.093 | 0.172 | 0.182 | 0.097 | 0.144 | 0.159 | 0.154 |
| K | 1.842 | 1.919 | 1.778 | 1.851 | 1.881 | 1.840 | 1.812 | 1.764 | 1.895 | 1.894 | 1.757 | 1.748 | 1.666 | 1.663 | 1.681 | 1.802 | 1.783 | 1.762 |
| OH | 4.000 | 4.000 | 4.000 | 4.000 | 4.000 | 4.000 | 4.000 | 4.000 | 4.000 | 4.000 | 4.000 | 4.000 | 4.000 | 4.000 | 4.000 | 4.000 | 4.000 | 4.000 |
| Tot. Cat. | 14.078 | 14.121 | 14.026 | 14.058 | 14.006 | 13.977 | 14.002 | 13.986 | 14.015 | 13.995 | 13.919 | 13.909 | 13.895 | 13.921 | 13.890 | 14.004 | 13.950 | 13.951 |
| XMg | 0.37 | 0.40 | 0.49 | 0.48 | 0.52 | 0.56 | 0.54 | 0.52 | 0.55 | 0.57 | 0.62 | 0.61 | 0.44 | 0.40 | 0.48 | 0.46 | 0.51 | 0.49 |
| XFe | 0.63 | 0.60 | 0.51 | 0.52 | 0.48 | 0.44 | 0.46 | 0.48 | 0.45 | 0.43 | 0.38 | 0.39 | 0.56 | 0.60 | 0.52 | 0.54 | 0.49 | 0.51 |

All Fe is assumed to be divalent

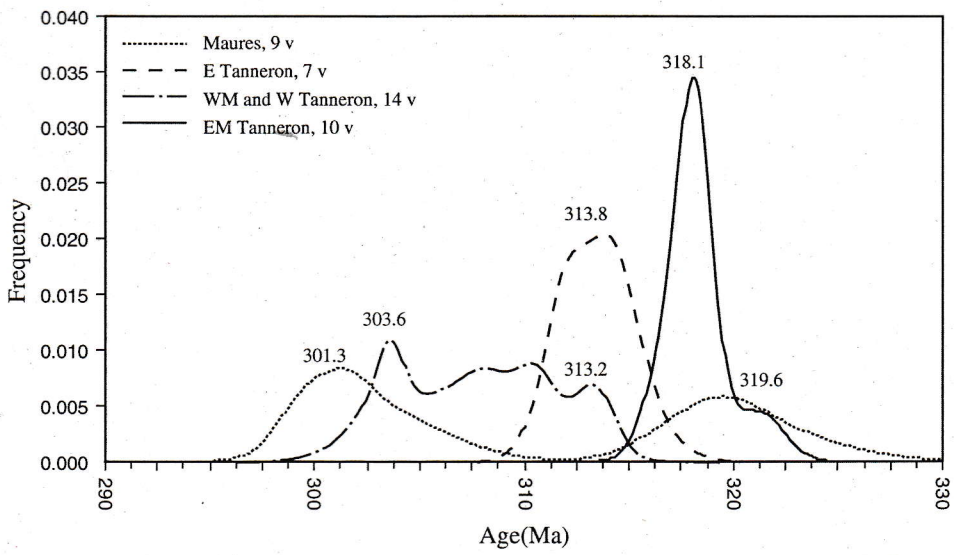


**Fig. 5** Frequency distribution of muscovite $^{40}Ar/^{39}Ar$ ages in the Tanneron Massif and in the Maures Massif from Morillon et al. (2000). Only muscovite ages from the Maures Massif are reported. The ages are shown at the $2\sigma$ level. In the Tanneron Massif, *E* eastern Tanneron, *WM* western part of the middle Tanneron, *W* western Tanneron, *EM* eastern part of the middle Tanneron

(2002) also observed plateau age scattering associated with disturbed age spectra (saddle-shaped and staircase shapes) in the context of granite emplacement (the Blond granite in the Massif Central, France). Saddle-shaped $^{40}Ar/^{39}Ar$ age spectra on muscovites from the granite as well as the age scattering are interpreted as the result of the circulation of hydrothermal fluids. The biotite $^{40}Ar/^{39}Ar$ ages from the host rock samples show older ages at increasing distances from the granite indicating that the emplacement of the granite occurred in relatively cold host rocks, e.g. at temperature lower than the isotopic closure of the K–Ar system in the biotite. Our results in the area of the Joyeuse fault are very similar to those obtained by Alexandrov et al. (2002) (1) excess or inherited $^{40}Ar$ is not likely because the ages are in the same order than those obtained in the southern Maures Massif (Morillon et al. 2000) and in the Tanneron (Demoux et al. 2008), (2) the $^{40}Ar/^{39}Ar$ plateau ages on muscovites from the surrounding rocks are younger in samples collected at decreasing distances of the Rouet granite (which displays the youngest age in the area), (3) even they allow plateau age calculation, spectra shapes and inconsistent ages in the same sample suggest post-isotopic closure disturbances in muscovite grains which could be the result of recrystallization processes. Thus, we propose that the scattering of the ages between 303 and 318 Ma on both side of the Joyeuse fault (e.g. at the boundary between the Western and the Middle Tanneron) is a consequence of the Rouet granite emplacement.

## Thermal doming of the Rouet magmatic complex

The youngest ages in the studied area were obtained in the Rouet granite (303.6 ± 1.2 Ma, sample TGD 08, Fig. 2) and in pegmatites or aplitic veins (samples FON 8, PEN 1 and PEN 2A). The biotite–cordierite Rouet granite intruded the surrounding metamorphic gneisses and the already solidified biotite–hornblende Prignonet tonalite. The Rouet granite is interpreted as the northern extension of the Plan-de-la-Tour granite in the Maures Massif, forming a single N–S elongated pluton emplaced in a pull-apart basin during the dextral wrenching of the Grimaud fault (Onezime et al. 1999). Geochronological data in both massifs are in agreement with this interpretation. Morillon et al. (2000) in the Maures Massif obtained $^{40}Ar/^{39}Ar$ plateau ages of 304.4 ± 2.7 ($1\sigma$) and 301.6 ± 1.1 Ma ($1\sigma$) on biotite from the Plan-de-la-Tour granite, and of 301.1 ± 0.6 Ma ($1\sigma$) on amphibole from the tonalite. Previous U–Pb ages from Moussavou (1998) in the Plan-de-la-Tour granite and in the tonalite were significantly older (see paragraph 3) but discordant U–Pb data in both cases suggest inherited zircons in the granite and tonalite. Recent U–Pb monazite dating (Demoux et al. 2008) yields an age at 302 ± 4 Ma for the Rouet granite. The $^{40}Ar/^{39}Ar$ ages in the Plan-de-la-Tour granite (Morillon et al. 2000) are consistent with the age of the Rouet granite and associated pegmatites and aplitic veins obtained in this study. These ages argue in favour of a rapid cooling of the magmatic body under the 350–450°C temperature interval at this period, that is around 15 Ma after the host rock samples (samples MON 1–19, ages from 317.4 ± 1.1 to 321.4 ± 1.1 Ma). In the field, a dome structure is spatially associated to the Rouet tonalite–granite intrusions. The metamorphic foliation displays an irregular trend all around the tonalite–granite complex and defined the dome-like Rouet antiform (Crevola in Toutin-Morin et al. 1994; Demoux et al. 2008). In the western and eastern side of this area the foliation planes are roughly submeridian and more or less steeply dipping, respectively, to the west and to the east. In contrast, in the northern and southern part of this area, the foliation planes are roughly sub equatorial and moderately to gently dipping, respectively to the north

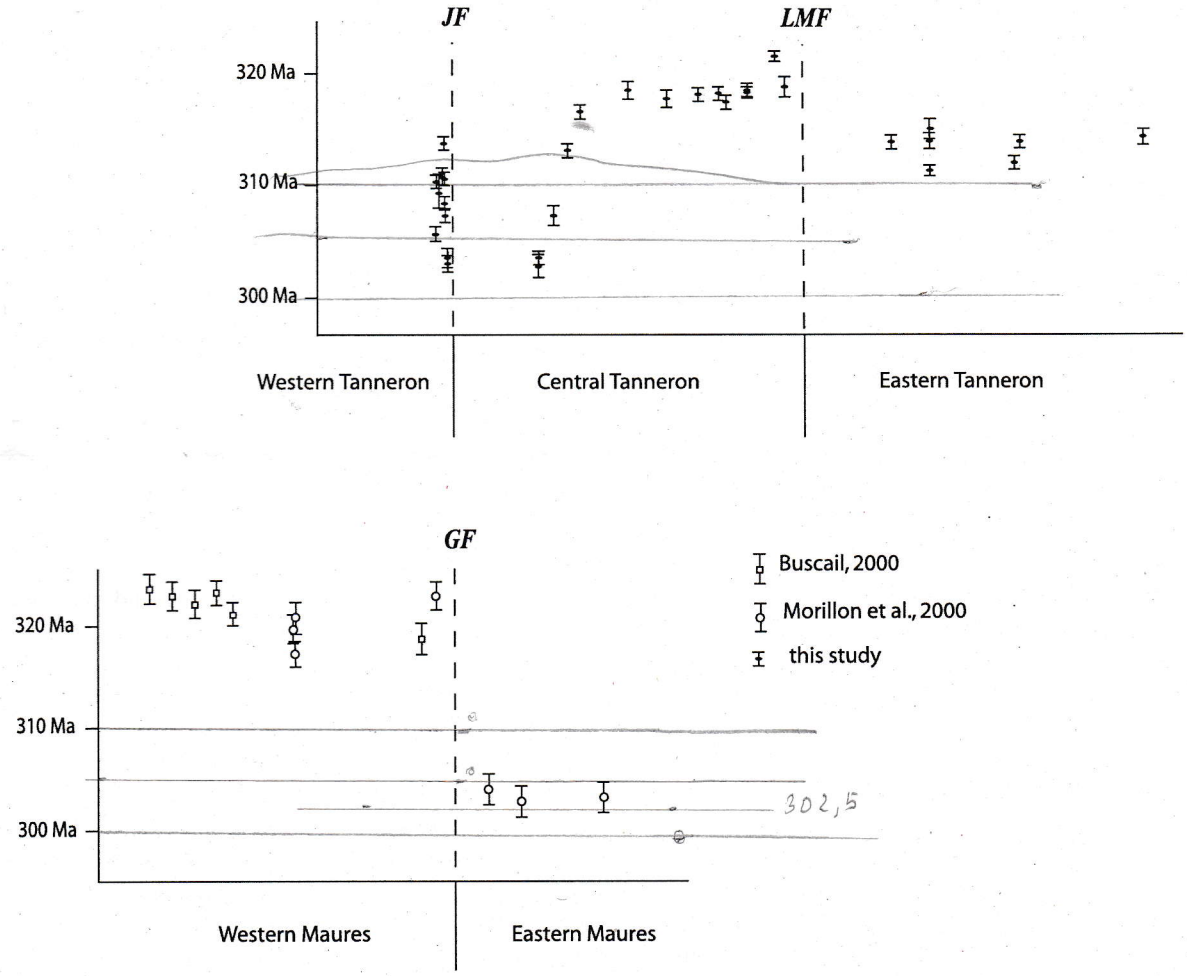


**Fig. 6** $^{40}Ar/^{39}Ar$ muscovite ages distribution across Tanneron and Maures Massif. The ages are shown at the $2\sigma$ level. *JF* Joyeuse fault, *LMf* La Moure fault, *GF* Grimaud fault

and to the south. The dome structure is also underlined by a mineral and stretching lineation which display a radial pattern. On the western border of the dome structure, kinematics indicators evidence normal shearing on the ductile to brittle Joyeuse fault, which is contemporaneous with the emplacement of the Rouet tonalite–granite intrusions and the opening of the Pennafort Stephanian basin. In this context, doming and local extension may be related to magmatic intrusions in the core of the Rouet anticline. Thus, we interpret the distribution of the $^{40}Ar/^{39}Ar$ ages, showing the age increase with the distance (Figs. 2, 6), as reflecting the presence of a thermal structure associated with the Rouet magmatic complex.

Numerical modelling for the thermal perturbation induced by intrusion of a pluton body in the country rocks shows that local thermal perturbation decays and migrates with time, so that rocks farther from the pluton cool earlier than rocks adjacent to the pluton (Sleep 1979). For large pluton bodies the thermal pulse may last for several millions years (Harrison and Clarke 1979). Large-scale folds of plurikilometer wavelengths can also produce a perturbation of the thermal surfaces (Sleep 1979; Burg and Podladchikov 1999; Mahéo et al. 2004). The heat transfer associated to melting invade the core of the anticline and migrate toward the surface. The rocks in anticline are eroded during exhumation and buried in syncline, where deposits concentrate. In the Tanneron Massif a similar model is supported by the occurrence of kilometer scale folding, location of magmatic complex in the core of the Rouet antiform and Stephanian detrital basins in the core of synforms (Figs. 1b, 2, 4).

On the western border of the dome structure, normal shearing on the Joyeuse fault is contemporaneous with the emplacement of the magmatic complex. Thus, doming is ascribed to fold amplification due to magmatic intrusions in the core of the Rouet anticline.

### Structural evolution and exhumation of the Maures-Tanneron Massifs

In the Maures Massif, Morillon et al. (2000) found two crustal blocks with distinct fast cooling paths at around 320 (western part) and 300 Ma (eastern part) separated by the Grimaud fault. If the Grimaud fault is extended in the Tanneron Massif by the Joyeuse fault, our results are not in agreement with this interpretation. However, this apparent disparity may be resolved by a comparison of two E–W cross-sections in the two massifs (Fig. 6). In the eastern block relative to the Grimaud fault in the Maures Massif, the whole formations cooled homogeneously between 300.2 ± 0.6 and 306.0 ± 2.4 Ma, which is consistent with the ages obtained around the Joyeuse fault in the middle Tanneron Massif. We propose that these ages correspond to the thermal influence of the Plan-de-la-Tour–Rouet magmatic complex, which hides the previous exhumation stage at 318 Ma only preserved in the eastern part of the middle Tanneron. The western block relative to the Grimaud fault, which shows older ages at around 320 Ma in the Maures Massif, is poorly exposed in the Tanneron Massif. In addition, the cooling paths between 318 Ma (eastern part of the middle Tanneron) and 314 Ma (eastern Tanneron) probably result from differential exhumation of distinct crustal blocks, controlled by the major ductile La Moure fault. This interpretation is in agreement with Morillon et al. (2000) to explain the age distribution in both sides of a fault.

These results outline the role of major faults, which separate crustal blocks during the exhumation processes, and also indicate that various processes contribute to the exhumation of the lower crust in the late stage of collision belts. In the Tanneron Massif, the exhumation of the lower crust is controlled during the first stage (between 318 and 314 Ma) by differential motion of tectonic blocks limited by ductile shear zones (La Moure fault and Joyeuse fault). The final exhumation at 303 Ma takes place within tectonic doming associated to magmatic intrusions, local ductile normal faulting and intracontinental basins opening. The thermal disturbance induced by the emplacement of the magmatic complex, which may be associated with fluid circulations, could explain the muscovite $^{40}Ar/^{39}Ar$ plateau age scatter observed in the host rock samples. This event could be related to orogen parallel shearing associated with crustal-scale strike-slip faults and regional folding (D3). A rather comparable evolution was described in the Himalayan syntaxis in Namche Barwa (Burg et al. 1998) and in South Karakorum (Mahéo et al. 2004), in Central Anatolia (Whitney et al. 2007) and in the West Carpathians (Jerabek et al. 2008), where doming in the core of crustal-scale folding and strike-slip faulting in a compressive regime control the heterogeneous exhumation of the lower crust.

## Conclusion

Detailed geochronological study performed in the Tanneron Massif revealed that late Variscan evolution lasted about 20 Ma during late Carboniferous from 320 to 300 Ma. The post-collisional exhumation is accommodated by crustal-scale ductile strike-slip faults associated with regional folding in the first stage from 320 to 310 Ma, and is followed by doming and anatexis in the core of antiformal structures at 305–295 Ma.

## References


Alexandrov P, Ruffet G, Cheilletz A (2002) Muscovite recrystallization and saddle-shaped $^{40}Ar/^{39}Ar$ age spectra: example from the blond granite (Massif Central, France). Geochim Cosmochim Acta 66:1793–1807. doi:10.1016/S0016-7037(01)00895-X

Arthaud F, Matte P (1966) Contribution à l'étude des tectoniques superposées dans la chaîne hercynienne: étude microtectonique des séries métamorphiques du massif des Maures (Var). C R Acad Sci Paris 262:436–439

Bard JP, Caruba C (1981) Les séries leptyno-amphiboliques à éclogites relictuelles et serpentinites des Maures, marqueurs d'une paléosuture varisque affectant une croûte amincie? C R Acad Sci Paris 292:611–614

Bard JP, Caruba C (1982) Texture et mineralogy d'une eclogite à disthène–saphirine–hyperstène–quartz en inclusion dans les gneiss migmatitites des Cavalières, massif de Ste Maxime (Maures, Var, France). C R Acad Sci Paris 294:103–106

Basso AM (1985) Le Carbonifère de Basse Provence (Sud–Est de la France). Doctorate thesis, University Aix-Marseille 1, France, p 319

Bellot JP, Bronner G, Laverne C (2000) Finite strain analysis and signification of ultramafic lenses from the Western Maures (SE France). Geodynamic implications. C R Acad Sci Paris 331:803–809

Bellot JP, Bronner G, Marchand J, Laverne C, Triboulet C (2002) Thrust and normal faulting in the Western Maures (SE France): evidence for geometric, kinematics and thermobarometry of the Cavalaire shear zone. Geol Fr 1:21–37

Bellot JP, Triboulet C, Laverne C, Bronner G (2003) Evidence for two burial/exhumation stages during the evolution of the Variscan belt, as exemplified by P-T-t-d paths of metabasites in distinct allochtonous units of the Maures Massif (SE France). Int J Earth Sci 92:7–26

Bouloton J, Goncalves P, Pin C (1998) Le pointement de péridotite à grenat-spinelle de La Croix-Valmer (Maures centrales): un cumulat d'affinité océanique impliqué dans la subduction éohercynienne? C R Acad Sci Paris 326:473–477

Burg JP, Podladchikov Y (1999) Lithospheric scale folding: numerical modeling and application to the Himalayan syntaxis. Int J Earth Sci 88:190–200. doi:10.1007/s005310050259

Burg JP, Van den Driessche J, Brun JP (1994) Syn- to post-thickening extension in the Variscan belt of Western Europe: mode and structural consequences. Geol Fr 3:33–51

Burg JP, Nievergelt P, Oberli F, Seward D, Davy P, Maurin JC, Zhizhong D, Meier M (1998) The Namche Barwa syntaxis: evidence for exhumation related to compressional crustal folding. J Asian Earth Sci 16:239–252. doi:10.1016/S0743-9547(98)00002-6

Buscail F (2000) Contribution à la compréhension du problème géologique et géodynamique du massif des Maures : le métamorphisme régional modélisé dans le système KFMASH : analyse paragénétique, chémiographie, thermobarométrie, géochronologie $^{40}Ar/^{39}Ar$. Ph.D. thesis, University of Montpellier, France

Buscail F, Leyreloup AF (1999) The collisional regional metamorphism in the Maures and Tanneron (south of France) area. A critical review. EUG10 meeting, Strasbourg, France, 28 March–1 April, J Conf Abstr, Oxford

Caruba C (1983) Nouvelles données pétrographiques, minéralogiques et géochmiques sur le massif métamorphique hercynien des Maures (Var, France): comparaison avec les segments varisques voisins et essais d'interprétation géotectonique. Doctorate thesis, University of Nice, France

Castonguay S, Ruffet G, Tremblay A, Féraud G (2001) Tectonometamorphic evolution of the southern Quebec Appalachians: $^{40}Ar/^{39}Ar$ evidence for the Middle Ordovician crustal thickening and Silurian–early Devonian exhumation of the internal Humber zone. Geol Soc Am Bull 113:144–160. doi:10.1130/0016-7606(2001)113<0144:TEOTSQ>2.0.CO;2

Cheilletz A, Ruffet G, Marignac C, Kolli O, Gasquet D, Féraud G, Bouillin JP (1999) $^{40}Ar/^{39}Ar$ dating of shear zones in the Variscan basement of Greater Kabilia (Algeria). Evidence of an Eo-Alpine event at 128 Ma (Hauterivian–Barremian boundary): geodynamic consequences. Tectonophysics 306:97–116. doi:10.1016/S0040-1951(99)00047-5

Corsini M, Ruffet G, Caby R (2004a) Alpine and late-Hercynian geochronological constraints in the Argentera Massif (Western Alps). Ecol Geol Helv 97:3–15

Corsini M, Bosse V, Demoux A, Billo S, Féraud G, Lardeaux JM, Rolland Y, Scharer U (2004b) Late orogenic HT-metamorphism and exhumation during ongoing convergence in the Hercynian Tanneron Massif France. Réunion des Sciences de la Terre, Strasbourg

Costa S, Rey P (1995) Lower crustal rejuvenation and growth during post-thickening collapse: insights from a crustal cross section through a Variscan metamorphic core complex. Geology 23:905–908. doi:10.1130/0091-7613(1995)023<0905:LCRAGD>2.3.CO;2

Crevola G (1977) Etude pétrographique et structurale de la partie orientale du massif du Tanneron (Provence cristalline). Doctorate thesis, University of Nice, France

Crevola G, Pupin J-P (1994) Crystalline provence: structure and variscan evolution. In: Keppie JD (ed) Pre-mesozoic geology in France and related areas. Springer, Berlin, pp 426–441

Crevola G, Pupin JP, Toutin-Morin N (1991) La Provence varisque: structure et évolution géologique anté-triasique. Sci Geol Bull 44:287–310

Dalrymple GB (1979) Critical tables for conversion of K–Ar ages from old to new constants. Geology 7(11):558–560. doi:10.1130/0091-7613(1979)7<558:CTFCOK>2.0.CO;2

Del Moro A, Di Simplicio P, Ghezzo C, Guasparri G, Rita F, Sabatini G (1975) Radiometric data and intrusive sequence in northern Sardinian batholith. Neues Jahrb Miner Abh 126:28–44

Demoux A, Scharer U, Corsini M (2008) Variscan evolution of the Tanneron Massif, SE-France, examined through U–Pb monazite ages. J Geol Soc Lond 165:467–478

Di Vincenzo G, Carosi R, Palmeri R (2004) The relationship between tectono-metamorphism evolution and argon isotope records in white mica: constraints from in situ $^{40}Ar/^{39}Ar$ laser analysis of the Variscan basement of Sardinia (Italy). J Petrol 45:1013–1043. doi:10.1093/petrology/egh002

Dunlap WJ (1997) Neocrystallization or cooling? $^{40}Ar/^{39}Ar$ ages of white micas from low-grade mylonites. Chem Geol 143:181–203. doi:10.1016/S0009-2541(97)00113-7

Dunlap WJ, Teyssier C, McDougall I, Baldwin S (1991) Ages of deformation from K–Ar and $^{40}Ar/^{39}Ar$ dating of white micas. Geology 19:1213–1216. doi:10.1130/0091-7613(1991)019<1213:AODFKA>2.3.CO;2

Echtler H, Malavielle J (1990) Extensional tectonics, basement uplift and Stephano-Permian collapse basin in a late Variscan metamorphic core complex (Montagne Noire, Southern Massif Central). Tectonophysics 177:125–138. doi:10.1016/0040-1951(90)90277-F

Faure JF (1995) Late orogenic Carboniferous extensions in the Variscan French Massif Central. Tectonics 14:132–153. doi:10.1029/94TC02021

Faure M, Monié P, Pin C, Maluski H, Leloix C (2002) Late Visean thermal event in the northern part of the French Massif Central: new $^{40}Ar/^{39}Ar$ and Rb–Sr isotopic constraints on the Hercynian syn-orogenic extension. Int J Earth Sci 91:53–75. doi:10.1007/s005310100202

Ferrara G, Ricci CA, Rita F (1978) Isotopic ages and tectonometamorphic history of the metamorphic basement of North-eastern Sardinia. Contrib Miner Petrol 68:99–106. doi:10.1007/BF00375451

Gardien V, Lardeaux JM, Ledru P, Allemand P, Guillot S (1997) Metamorphism during the late orogenic extension: insights from the French Variscan belt. Bull Soc Geol Fr 168(3):271–286

Harrison TM, Clarke GKC (1979) A model of the thermal effects of igneous intrusion and uplift as supplied to Quottoon pluton, British Columbia. Can J Earth Sci 6:411–420

Innocent C, Michard A, Guerrot C, Hamelin B (2003) U–Pb zircon age of 548 Ma for the leptynites (high-grade felsic rocks) of the central part of the Maures Massif. Geodynamic significance of the so-called leptyno-amphibolitic complexes of the Variscan belt of western Europe. Bull Soc Geol Fr 174:585–594. doi:10.2113/174.6.585

Jerabek P, Faryadi WS, Schulmann K, Lexa O, Tajcmanova L (2008) Alpine burial and heterogeneous exhumation of Variscan crust in the West Carpathians: insight from thermodynamic and argon diffusion modelling. J Geol Soc Lond 165:479–498

Le Marrec A (1976) Reconnaissance pétrographique et structurale des formations cristallophylliennes catazonales du Massif de Sainte-Maxime (quart NE du massif varisque des Maures, Var, France). Thesis, University of Aix-Marseille III

Mahéo G, Pêcher A, Guillot S, Rolland Y, Delacourt C (2004) Exhumation of Neogene gneiss domes between oblique crustal boundaries in south Karakorum (northwest Himalaya, Pakistan). Geol Soc Am Special paper 380:141–154

Malavieille J (1993) Late orogenic extension in mountain belts: insights from the Basin and Range and the late Paleozoic Variscan belt. Tectonics 12:1115–1130. doi:10.1029/93TC01129

Maluski H (1972) Etude $^{87}Rb/^{87}Sr$ du massif granitique de Plan-de-la-Tour (Maures). C R Acad Sci Paris 274:520–523

Maquil R (1976) Contribution à l'étude pétrographique et structurale de la région SE du massif des Maures (Var, France). Ann Soc Geol Belg 99:601–613

Matte P (2001) The variscan collage and orogeny (480–290 Ma) and the tectonic definition of the Armorica microplate: a review. Terra Nova 13:117–121. doi:10.1046/j.1365-3121.2001.00327.x

McDougall M, Harrison TM (1999) Geochronology and thermochronology by the $^{40}Ar/^{39}Ar$ method. Oxford University Press, New York

Monié P, Maluski H (1983) Données géochronologiques $Ar^{39}$–$Ar^{40}$ sur le socle anté-Permien du massif de l'Argentera-Mercantour (Alpes-Maritimes, France). Bull Soc Geol Fr 7:247–257

Morillon AC (1997) Etude thermo-chronométrique appliquée aux exhumations et contexte orogénique: le Massif des Maures (France) et Les Cordillères Bétiques (Espagne). Thesis, University of Nice, pp 289

Morillon AC, Féraud G, Sosson M, Ruffet G, Crévola G, Lerouge G (2000) Diachronous cooling on both side of a major strike-slip fault in the Variscan Maures Massif (SE France), as deduced from a detailed $^{40}Ar/^{39}Ar$ study. Tectonophysics 321:103–126. doi:10.1016/S0040-1951(00)00076-7

Moussavou M (1998) Contribution à l'histoire thermo-tectonique Varisque du Massif des Maures, par la typologie du zircon et la géochronologie U/Pb sur minéraux accessoires. Thesis, Montpellier, 179

Mulch A, Cosca MA, Handy MR (2002) In-situ UV-laser $^{40}Ar/^{39}Ar$ geochronology of a micaceous mylonite : an example of defect-enhanced argon loss. Contrib Miner Petrol 142:738–752

Odin C, Odin GS (1990) Echelle numérique des temps géologiques, Géochronique 35

Onezime J, Faure M, Crevola G (1999) Petro-structural analysis of the Rouet–Plan-de-la-Tour granitic complex (Maures and Tanneron Massifs, Var, France). C R Acad Sci 328(11):773–779

Paquette JL, Ménot RP, Peucat JJ (1989) REE, Sm–Nd and U–Pb zircon study of eclogites from the Alpine external Massifs (Western Alps): evidence for crustal contamination. Earth Planet Sci Lett 96:181–189. doi:10.1016/0012-821X(89)90131-3

Paquette JL, Ménot RP, Pin C, Orsini JB (2003) Episodic and short-lived granitic pulses in a post-collisional setting: evidence from precise U–Pb zircon dating through a crustal cross-section in Corsica. Chem Geol 198:1–20. doi:10.1016/S0009-2541(02)00401-1

Roddick JC (1983) High precision intercalibration of $^{40}Ar/^{39}Ar$ standards. Geochim Cosmochim Acta 47:887–898. doi:10.1016/0016-7037(83)90154-0

Roubault MP, Bordet FL, Sonet J, Zimmermann JL (1970) Ages absolus des formations cristallophylliennes des Massifs des Maures et du Tanneron. C R Acad Sci 271:1067–1070

Rubatto D, Schaltegger U, Lombardo B, Colombo F, Compagnoni R (2001) Complex Paleozoic magmatic and metamorphic evolution in the Argentera Massif (Western Alps) resolved with U–Pb dating. Schweizerische Minér Petrogr 81:213–228

Ruffet G, Féraud G, Amouric M (1991) Comparison of $^{40}Ar/^{39}Ar$ conventional and laser dating of biotites from the North Tregor Batholith. Geochim Cosmochim Acta 55:1675–1688. doi:10.1016/0016-7037(91)90138-U

Seyler M (1975) Pétrologie et lithostratigraphie des formations cristallophylliennes dans la chaîne de la Sauvette (Maures, Var, France). Thesis, Université of Nice

Seyler M (1982) Caractères pétrographiques et chimiques des métagabbros de la partie centrale du massif des Maures (Var). Bull Soc Geol Fr 24:717–725

Sleep NH (1979) A thermal constraint on the duration of folding with references to Acadian geology, New England (USA). J Geol 87:583–589

Soula JC, Debat P, Brusset S, Bessière G, Christophoul F, Déramond J (2001) Thrust-related, diapiric, and extensional doming in a frontal orogenic wedge: example of the Montagne Noire, Southern French Hercynian belt. J Struct Geol 23:1677–1699. doi:10.1016/S0191-8141(01)00021-9

Steiger RH, Jäger E (1977) Submission on geochronology: convention in the use of decay constants in geo and cosmochronology. Earth Planet Sci Lett 36:359–362. doi:10.1016/0012-821X(77)90060-7

Toutin-Morin N, Crevola G, Giraud JD, Brocard C, Dardeau G, Bulard PF, Dubar M, Meinesz A, Bonijoly D(1994) Carte géologique Fréjus-Cannes à 1/50 000, 2ème édn (1024) carte et notice. BRGM Orléans

Turner G, Huneke JC, Podosek FA, Wasserburg GJ (1971) $^{40}Ar/^{39}Ar$ ages and cosmic ray exposure ages of Apollo 14 samples. Earth Planet Sci Lett 12:19–35. doi:10.1016/0012-821X(71)90051-3

Vauchez A, Bufalo M (1985) La limite Maures occidentales-Maures orientales (Var, France): un décrochement majeur entre deux provinces structurales très contrastées. C R Acad Sci Paris 301(14):1059–1062

Vauchez A, Bufalo M (1988) Charriage crustal, anatexie, et décrochements ductiles dans les Maures orientales (Var, France) au cours de l'orogenèse varisque. Geol Rundsch 77:45–62. doi:10.1007/BF01848675

Villa IM (1998) Isotopic closure. Terra Nova 10:42–47. doi:10.1046/j.1365-3121.1998.00156.x

Whitney DL, Teyssier C, Heizler MT (2007) Gneiss domes, metamorphic core complexes, and wrench zones: thermal and structural evolution of the Nigde Massif, central Anatolia. Tectonics 26:1–23. doi:10.1029/2006TC002040